Nanoscale

Accepted Manuscript

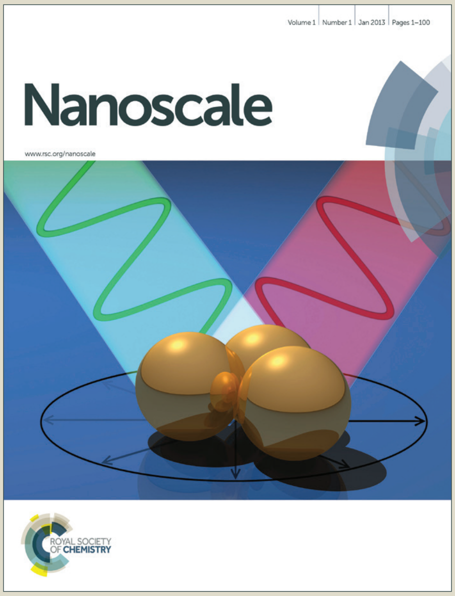

ROYAL SOCIETY OF CHEMISTRY

www.rsc.org/nanoscale

Nanoscale RSCPublishing

PAPER

Cite this: DOI: 10.1039/x0xx00000x

Structural transformation of carbon-supported Pt_3Cr nanoparticles from disordered to ordered phase as durable oxygen reduction electrocatalyst

Liangliang Zou[a, b], Jun Li [a, b], Ting Yuan[a, *], Yi Zhou[a], Xuemei Li[a] and Hui Yang[a,*]

Received 00th xx 2014,
Accepted 00th xx 2014

DOI: 10.1039/x0xx00000x

www.rsc.org/nanoscale

The sluggish oxygen reduction kinetics and insufficient durability of cathode catalysts restrict the practical application of proton exchange membrane fuel cells. This study focuses on the structural transformation of carbon-supported Pt_3Cr from a disordered to an ordered phase and on the effect of such structural transformation on oxygen reduction reaction (ORR) activity and durability. X-ray diffraction and transmission electron microscopy results confirm the formation of carbon-supported Pt_3Cr intermetallic nanoparticles with a mean particle size of ca. 7.2 nm. Line scanning EDX reveals that the practical Pt/Cr atomic ratio is approximately 3:1. X-ray photoelectron spectroscopy results indicate that the proportion of metallic Pt increases while the binding energy of Pt 4f decreases with such structural transformation. The Pt_3Cr/C intermetallic nanoparticles exhibit enhanced mass and specific activities toward the ORR compared with commercial Pt/C but slightly lower mass activity than the disordered Pt_3Cr/C alloy nanoparticles. After accelerated durability test for 5000 cycles, the Pt_3Cr intermetallic nanoparticles displayed negligible decay in ORR mass activity; however the ORR mass activity on disordered Pt_3Cr alloy decreases to ca. 50%. Much enhanced durability of the Pt_3Cr/C intermetallic nanoparticles toward the ORR is definitely caused by the much higher structural and compositional stabilities of the Pt_3Cr/C intermetallic nanoparticles than that of the disordered Pt_3Cr/C alloy nanoparticles, suggesting that the Pt_3Cr intermetallic nanoparticles may serve as highly active and durable ORR electrocatalysts for practical application.

1 Introduction

Proton exchange membrane fuel cells (PEMFC) have recently been considered as the next-generation power supply because of their high-energy density, high-energy conversion efficiency, low pollution, and relatively low working temperatures.[1, 2.] However, several technical challenges, such as the high cost of Pt-based electrocatalysts, the sluggish kinetics of cathode reaction, and the insufficient durability of the catalysts, should be addressed for their practical applications.[3, 4] Pt alloyed with transition metals (e.g., Fe[5], Co[6, 7], Ni[8], Mn[9], and Cr[10]) and low-content Pt electrocatalysts (e.g., core-shell[11, 12] and hollow structure [13]), have proved to be a better alternative for supported Pt catalysts in terms of electrocatalytic activity and cost. Mukerjee et al.[14] investigated various Pt bimetallic alloys supported on carbon and found a two- to three-fold increase in the oxygen reduction reaction (ORR) activity under PEMFC operating conditions. However, the stability of the Pt-based alloy catalysts does not meet the requirement for practical application because of possible dissolution of transition metals within the catalysts for long-term operation.[15]

Recent studies have found that Pt-based intermetallic compounds not only reduce the cost of the catalysts, but also exhibit enhanced ORR activity and durability, compared with their disordered alloys, because they allow a greater degree of control over their composition, structural, and electronic properties.[16] Abruna et al.[17]synthesized carbon-supported Pt_3Co intermetallic nanoparticles through an impregnation method followed by heat treatment. The results of the electrochemical tests of the Pt-based nanoparticles with Pt layer on the surface and Pt–Co intermetallic compounds as the core show that the electrocatalysts exhibited enhanced activity and stability for the ORR. Botton et al.[18] found that Pt_3Fe_2 intermetallic nanoparticle catalysts present a static core-dynamic shell regime, in which the Pt_3Fe_2 core is virtually intact, and the Pt

---

[a] *Shanghai Advanced Research Institute, Chinese Academy of Sciences (CAS), Shanghai 201210,China*
[b] *University of the CAS, Beijing 100039, China*

**Corresponding authors*
Fax: +86-21-20325112
E-mails: yangh@sari.ac.cn & yuant@sari.ac.cn

†. Electronic Supplementary Information (ESI) available. See DOI:10.1039/b000000x/

shell suffers continuous enrichment during long-term cycling. Xia et al.[19] also verified that using carbon-supported Pt_3Fe and PtFe intermetallic nanoparticles enhances the activity and durability of the ORR electrocatalysts. Moreover, $PtBi_2$[20], PtNi [21], PtSn[22], PtPb[23-25], and Pt_3Zn[26] intermetallic nanoparticles have been reported as promising candidates for fuel-cell catalysts.

Among the various Pt-based alloy catalysts used for the ORR, the Pt–Cr alloy is more stable in acidic and oxidizing media at high temperature[10], whereas the Pt–Cu and Pt–Fe alloys are unstable under fuel-cell operating conditions. The Pt–Cr alloy appears to be a promising ORR catalyst.[27, 28] Additionally, Yang et al. found that the presence of $Pt_{1.5}Cr_{2.5}$ super lattice may facilitate an improvement in ORR activity.[29] Thus, Pt_3Cr/C intermetallic electrocatalysts could be used as active and durable ORR catalysts for PEMFCs. In the present study, carbon-supported Pt_3Cr disordered alloy nanoparticles (i.e., solid solution) were first synthesized. The structural transformation of carbon-supported Pt_3Cr from a disordered to an ordered phase and the effect of such structural transformation on the ORR activity and durability were investigated.

2 Experimental

2.1 Materials

Sodium chloroplatinate ($Na_2PtCl_6 \cdot 6H_2O$) and chromium chloride ($CrCl_3$) were purchased from Aldrich, and sodium acetate (CH_3COONa, AR) and methanol (CH_3OH, AR) were supplied by Sinopharm Chemical Reagent Co., Ltd. All reactants were used as received.

2.2 Methods

Carbon-supported disordered Pt_3Cr/C (D-Pt_3Cr/C) was synthesized according to a previously reported method[29, 30]. The carbonyl complex was synthesized by adding 285 mg $Na_2PtCl_6 \cdot 6H_2O$, 27 mg $CrCl_3$, and 336 mg CH_3COONa into 45 mL methanol solution kept at 55 °C for at least 8 h under CO atmosphere. Then, 435 mg KB-600 was added into the as-prepared solution stirred at 55 °C for 8 h. Subsequently, the solvent was removed by purging N_2 at 70 °C. The as-prepared D-Pt_3Cr/C catalysts were then annealed at 400 °C to 500 °C under H_2/N_2 atmosphere for 5 h to obtain D-Pt_3Cr/C. Then, the D-Pt_3Cr/C was subjected to heat treatment at 700 °C to 800 °C under H_2 atmosphere for 3h to obtain carbon-supported Pt_3Cr intermetallic compound nanoparticles, denoted as O-Pt_3Cr/C.

2.3 Physical characterization

The composition of the catalysts was measured by an IRIS Advantage inductively coupled plasma–atomic emission spectroscopy (ICP–AES) system (Thermo America). Powder X-ray diffraction (XRD) measurements were conducted using a Bruker AXS D8 Advance powder X-ray diffractometer with a Cu Kα (λ = 1.5418 Å) radiation source, operating at 40 kV and 40 mA. Diffraction patterns were collected at a scanning rate of 2° min^{-1} and with a step size of 0.02°. X-ray photoelectron spectroscopy was conducted using a Kratos AXIS Ultra^{DLD} with Al Kα radiation. The binding energies (BEs) derived from XPS measurements were referenced to the C_{1s} BE at 284.45 eV. Transmission electron microscopy (TEM) images were obtained with a JEOL 2100F at an accelerating voltage of 200 kV.

2.4 Electrochemical characterization

Porous electrodes were prepared as previously described.[31] A measured volume (ca. 3μL) of ultrasonic treated ink, which included 10 mg catalyst, 2.8 mL water, and 0.2 mL Nafion solution (5 wt.%, Aldrich), was transferred onto a freshly polished glassy carbon disk (GC, 3 mm in diameter) and left to dry overnight at room temperature. Electrochemical measurements (all conducted at 25 ± 1 °C) were performed using CHI 730B Potentiostat/Galvanostat and a conventional three-electrode electrochemical cell. The counter electrode used was a glassy carbon plate, and a saturated calomel electrode was employed as the reference electrode. Accelerated durability test (ADT) was conducted on a Solartron SI1287 Potentiostat/Galvanostat. Potentials quoted herein are with respect to the reversible hydrogen electrode (RHE). The electrochemical surface areas (ECSAs) of the catalysts were determined by hydrogen adsorption or desorption area and CO_{ad} oxidation in CO stripping voltammetry. The oxidation charge for a monolayer of adsorbed H and CO on a Pt surface was assumed to be 210 and 420 $\mu C cm^{-2}$, respectively.[32] High-purity nitrogen or oxygen was used for deaeration of the solutions, and during the measurement, a gentle gas flow was maintained above the electrolyte solution.

3 Results and discussion

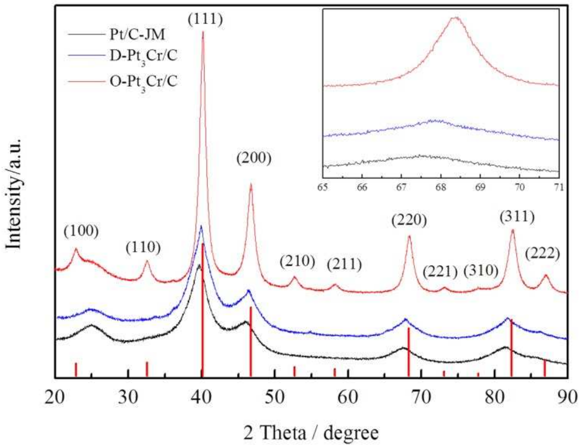

Fig. 1 XRD patterns of the Pt/C-JM, D-Pt_3Cr/C and O-Pt_3Cr/C catalysts; the inset shows the enlarged region of (220) planes.

Figure 1 displays the XRD patterns of Pt/C–JM, D–Pt_3Cr/C, and O–Pt_3Cr/C. The broad peak at around 25° for all materials is attributable to carbon support. The other five main characteristic peaks for the D-Pt_3Cr/C are face-centered-cubic (fcc) crystalline Pt, namely, the planes (111), (200), (220), (311), and (222), demonstrating that it is mainly single-phased, with an fcc disordered structure. The diffraction peaks for D-Pt_3Cr/C are shifted to higher 2θ values compared with those for Pt/C-JM, which can be clearly observed in the inset of Figure 1, indicating that metallic Cr is incorporated into the Pt fcc structure to form an alloy phase with lattice contraction.[30]

Table 1 Characterization of the Pt/C-JM, D-Pt_3Cr/C and O-Pt_3Cr/C catalysts

Sample	Lattice parameter (nm)	Particle size (nm)	$ECSAs_H$ (m^2g^{-1})	$ECSAs_{CO}$ (m^2g^{-1})	MA ($mAmg^{-1}$)		SA (μAcm_{Pt}^{-2})	
					0.85V	0.90V	0.85V	0.90V
Pt/C-JM	0.3916	3.5	66	67	12.4	2.1	17.7	3.0
D-Pt_3Cr/C	0.3895	3.1	70	75	30.4	5.7	40.5	7.6
O-Pt_3Cr/C	0.3876	7.2	32	35	23.2	4.3	63.5	12.3

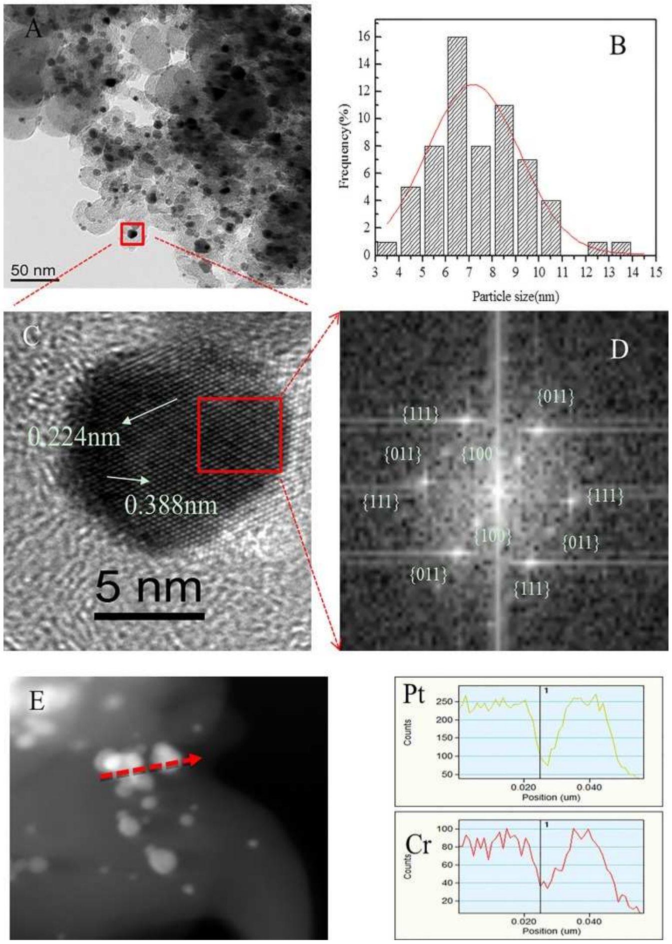

Fig. 2 (A) TEM images of O-Pt_3Cr/C and (B) its particle size distribution; (C) HRTEM image of a single Pt_3Cr intermetallic nanoparticle in A; (D) FFT of (C); (E) EDS line scanning of Pt_3Cr nanoparticles with Pt and Cr distributions.

Except for the abovementioned peaks, the XRD pattern of O-Pt_3Cr/C presents additional (100), (110), (210), (221), and (310) peaks, which are characteristics of an ordered intermetallic Pt_3Cr phase. These peaks are matched well with the standard PDF card of the $CrPt_3$ intermetallic phase (JCPDS No. 65-6577), suggesting the formation of Pt_3Cr intermetallic compound nanoparticles. The lattice parameter, obtained fromthe (220) diffraction peak, and the mean particle size, calculated using the Debye–Scherrer equation based on the peak width of the (220) reflection, are provided in Table 1.

The TEM image of O-Pt_3Cr/C and its corresponding particle size distribution are presented in Figs. 2A and 2B, respectively, which show that the Pt_3Cr nanoparticles are well dispersed on the surface of carbon support. The obtained average particle size for the O-Pt_3Cr/C is approximately 7.2 nm, which is in fairly good agreement with the XRD result (Table 1).A typical HRTEM image in Fig. 2C and Fourier fast transform (FFT) analysis in Fig. 2D clearly indicate the appearance of lattice planes for O-Pt_3Cr, which again verifies the formation of Pt_3Cr intermetallic compounds. The lattice planes of the focused nanocrystal with spacing distances of 0.224 and 0.388 nm can be indexed as the (111) and (100) planes of O–Pt_3Cr nanocrystals. EDX line scanning is employed to investigate the composition of O–Pt_3Cr/C (Fig. 2E). The figure shows that Pt and Cr are uniformly distributed along the scanning line, and that the intensity ratio of Pt/Cr is almost 3:1. This result indicates that the practical atomic ratio of Pt/Cr is approximately 3:1, which is nearly similar to the nominal composition.

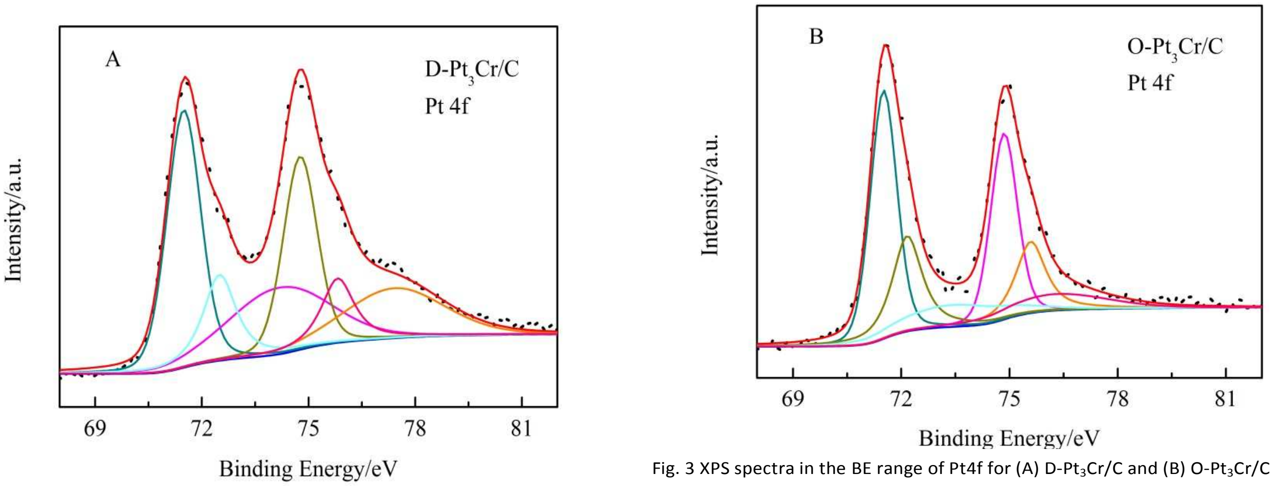

Fig. 3 XPS spectra in the BE range of Pt4f for (A) D-Pt$_3$Cr/C and (B) O-Pt$_3$Cr/C

Table 2 BEs for Pt 4f and atomic percentages (AP, %) of different Pt species

	D-Pt$_3$Cr/C				O-Pt$_3$Cr/C			
	Initial		After ADT		Initial		After ADT	
	BE	AP	BE	AP	BE	AP	BE	AP
Pt(0)	71.49	46.1	71.42	31.6	71.44	55.6	71.07	43.4
Pt(II)	72.50	18.8	71.95	30.6	72.22	28.1	71.57	35.4
Pt(IV)	74.19	35.1	72.72	37.8	73.66	16.3	73.06	21.2

To explore the electronic properties of the Pt$_3$Cr structural transformation from disordered to ordered phase, both samples were subjected to XPS analysis. Figure 3 shows the Pt 4f XPS spectra of D-Pt$_3$Cr/C and O-Pt$_3$Cr/C in the BE ranges between 68 and 82 eV for Pt 4f. Each curve can be deconvoluted into three pairs of peak doublets (Table 2). The BEs for the pairs are located at 71.49, 74.83; 72.50, 75.82; and 74.19, 77.41 eV for D-Pt$_3$Cr/C, which are respectively assigned as Pt(0), Pt(II), and Pt(IV), and 71.44, 74.78; 72.22, 75.62; and 73.66, 76.37 eV for O-Pt$_3$Cr/C. The obtained BEs for both Pt$_3$Cr/C samples are higher than those for the Pt bulk.[33, 34] The BEs of O-Pt$_3$Cr/C are smaller than those of D-Pt$_3$Cr/C, which could be have resulted from the strong interaction between Pt and Cr within O-Pt$_3$Cr/C and to the particle size effect such that the BE shifts to higher energy with the decreased particle size.[35] The atomic percentages of Pt(0), Pt(II), and Pt(IV) in Table 2 indicate that the presence of metallic Pt is its major state in the O-Pt$_3$Cr/C relative to that in the D-Pt$_3$Cr/C, suggesting an increased oxidation resistance of Pt in an ordered intermetallic phase, which would lead to an enhancement in ORR kinetics[33].

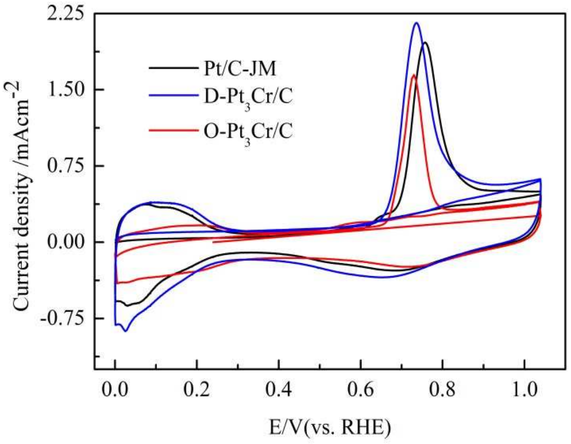

Fig. 4 CO-stripping voltammograms of the Pt/C-JM, D-Pt$_3$Cr/C and O-Pt$_3$Cr/C catalysts in 0.1 M HClO$_4$ at a scan rate of 20 mVs^{-1}

To obtain more insights into surface microstructures and real surface area of Pt for bimetallic catalysts, the CO-stripping voltammograms of the Pt/C-JM, D-Pt$_3$Cr/C, and O-Pt$_3$Cr/C catalysts are shown in Figure 4. The hydrogen adsorption/desorption and peroxidation/reduction peaks of the Pt surface on Pt/C-JM are clearly observed, indicating the presence of polycrystalline Pt. No well-defined hydrogen adsorption/desorption peaks are found on the carbon-supported disordered/ordered Pt$_3$Cr alloys, which indicates the formation of well-alloyed Pt-Cr alloys. Moreover, the onset and peak potentials of COad oxidation on the Pt$_3$Cr/C catalysts are slightly shifted to more negative potential than those on Pt/C-JM, demonstrating that the Pt$_3$Cr alloy electrocatalysts exhibit better CO tolerance. By integrating the hydrogen desorption and CO_{ad} oxidation areas, the $ECSAs_H$ and $ECSAs_{CO}$ can be obtained (Table 1). The $ECSAs_{CO}$ for all samples are slightly larger than $ECSAs_H$. However, the change in both ECSAs shows a similar trend.

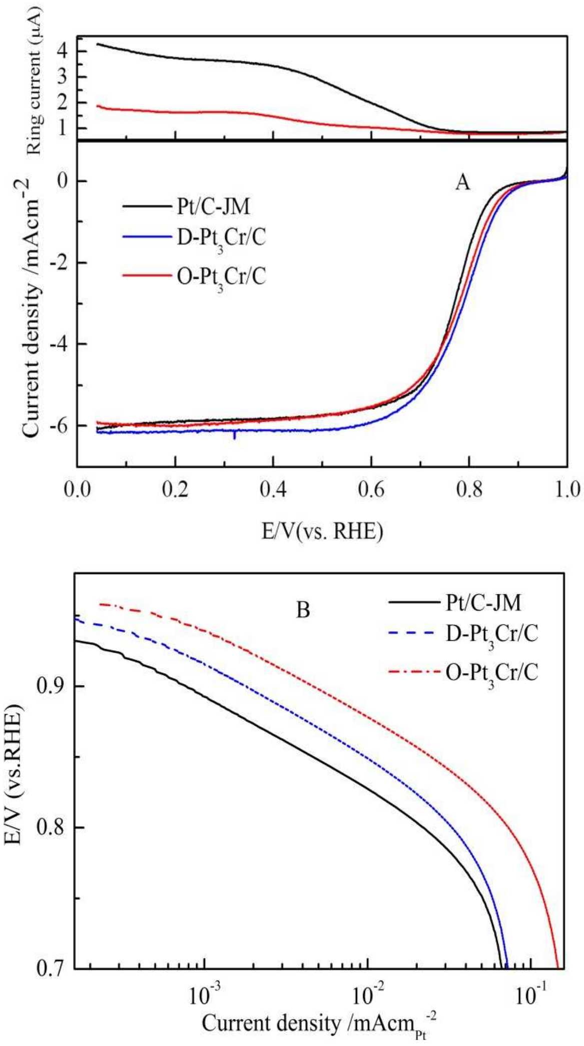

Fig. 5 (A) Linear scan voltammograms of the Pt/C-JM, D-Pt_3Cr/C and O-Pt_3Cr/C in O_2-saturated 0.1M $HClO_4$ solution at scan rate of 5mVs^{-1} and at a rotation speed of 1600 rpm .The ring currents, RRDE data, for hydrogen peroxide production are contrasted.; (B) Tafel plots for the ORR on the three catalysts, current density are normalized to the real surface area of platinum within the catalysts

Figure 5A shows the comparison of the ORR on the Pt/C–JM, D–Pt_3Cr/C, and O–Pt_3Cr/C under similar experimental conditions. The ORR on all three catalysts is diffusion-controlled when the potential is less than 0.7 V and under mixed diffusion kinetics control in the potential region between 0.7 and 0.85 V. In the Tafel (potential region higher than 0.85 V) and mixed potential regions, the ORR activities of all catalysts are identical with respect to the mass activity (MA) of the total metal loading. The obtained MA and specific activity (SA) of the ORR on the three samples are also listed in Table 1. The MA based on Pt decreases in the order of D-Pt_3Cr/C>O-Pt_3Cr/C> Pt/C-JM. Figure 5B shows the Tafel plots of the ORR on the three catalysts based on their $ECSAs_{CO}$. The obtained Tafel slopes at potentials of > 0.85 V for the Pt/C-JM, D-Pt_3Cr/C and O-Pt_3Cr/C catalysts are 65, 68, and 69 mV decade^{-1}, respectively. Within the fitting error, the Tafel slope does not show any dependence on the compositional and structural parameters of the catalysts. Thus, the reaction pathway and the rate-determining step are similar in all three catalysts. Further comparison in ORR SA indicates that the SA increases in the order of Pt/C-JM<D-Pt_3Cr/C<O-Pt_3Cr/C in the Tafel region (Table 1). A significant enhancement in ORR SA on the O-Pt_3Cr/C can be attributable to the electronic and ordered structural effects.[29, 36]

For an efficient ORR catalyst, quantifying the relative formation rates of water (four-electron pathway) or hydrogen peroxide (two-electron pathway) is important because peroxide is corrosive toward carbon materials and Nafion resin and can cause the oxidation destruction of active and defective sites in fuel-cell catalysts and supports.[37] Rotating ring-disk electrode (RRDE) data shown in Figure 5A are illustrative of the ORR pathway on Pt/C-JM and O-Pt_3Cr/C catalysts. The ring current is found to be negligible compared with the disk current for potentials above 0.80 V, indicating that the ORR proceeds nearly without peroxide production. The ring current increases, starting from potentials lower than 0.75 V, and the amount of peroxide formed on the O-Pt_3Cr/C catalyst is slightly higher than that on the Pt/C. The fraction of peroxide, at a typical fuel cell operating potential of 0.70 V, can be calculated.[37] The fractions for the peroxide production on the Pt/C-JM and O-Pt_3Cr/C catalysts are 0.92% and 1.16%, respectively, revealing negligible peroxide production. Thus, the ORR on O-Pt_3Cr/C undergoes a four-electron process leading to water formation.

The Pt-based alloy catalyst is well known as an alternative cathode material because of its high activity for the ORR. However, the durability of such alloys should be significantly improved. In this study, the durability of the catalysts was evaluated by potential cycling between 0.05 and 1 V/RHE for 5000 cycles in an N_2-saturated 0.1 M HClO4 and at 50 mVs^{-1}. The cyclic voltammograms (CVs) in N_2-saturated and LSVs in O_2-saturated 0.1 M $HClO_4$ of catalysts for initial and 5000th cycle are shown in Figure 6. The ECSA of Pt/C-JM decreases to 77% of the initial value after 5000 cycles, and the MA decreases to 26.4% of the initial MA at 0.85 V. The significant reduction in both ECSA and MA could have been caused by the possible aggregation of Pt nanoparticles and/or dissolution of Pt species. Such relatively poor durability has been reported in many studies.[39]The hydrogen adsorption/desorption peaks for D-Pt_3Cr/C become prominent with continued cycling, and the ECSA of D-Pt_3Cr/C decreases by 10%, indicating that Pt enrichment on the surface caused by the Cr is leaching away from the disordered Pt_3Cr alloy nanoparticles. Moreover, the ORR MA decreases by a factor of approximately 50% at 0.85 and 0.9 V after ADT, indicating that the disordered Pt_3Cr alloy catalyst is more stable than the Pt/C catalyst. Meanwhile, the currents of well-defined hydrogen adsorption/desorption and Pt oxide peaks of O-Pt_3Cr/C slightly increase after 5000 cycles. The Cr/Cr oxides on the catalyst surface may have dissolved with the potential cycling. The ORR MA of O-Pt_3Cr/C slightly decreases, and after 5000 cycles, the ORR MA is higher on O-Pt_3Cr/C than on D-Pt_3Cr/C, demonstrating that durability considerably improved after the disordered Pt_3Cr alloy phase transformed into the ordered Pt_3Cr alloy phase.

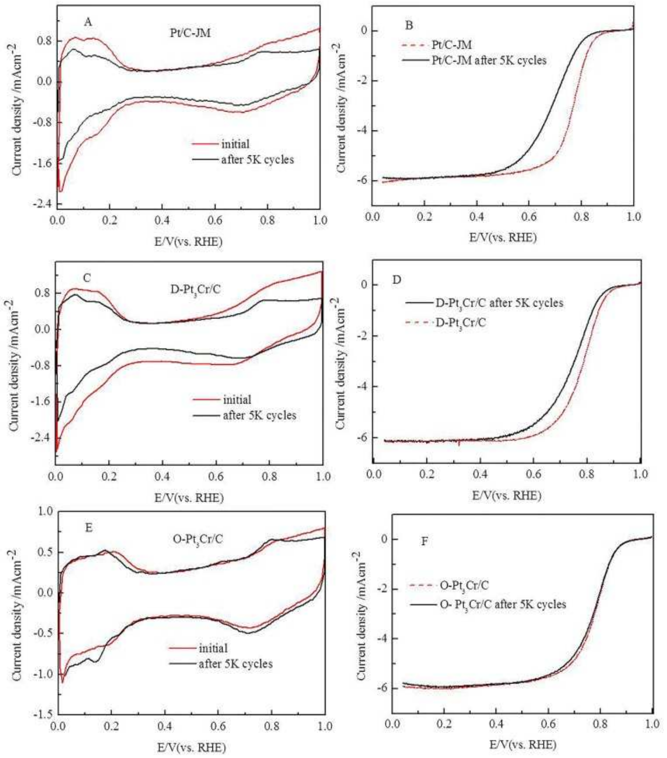

Fig. 6 Cyclic voltammetry of Pt/C-JM (A), D-Pt_3Cr/C (C) and O-Pt_3Cr/C (E) in N_2 saturated 0.1M $HClO_4$ solution before and after 5K cycles, as indicated, at a scan rate of $50 mVs^{-1}$; Comparative ORR activities of Pt/C-JM(B), D-Pt_3Cr/C (D) and O-Pt_3Cr/C(F) before and after 5K cycles in O_2 saturated 0.1M $HClO_4$ solution at a scan rate of $5 mVs^{-1}$.

ICP-AES was employed to analyse the possible dissolution of Cr species in the solution after ADT. Cr species are detected in the solution after ADT for both D-Pt_3Cr/C and O-Pt_3Cr/C. Given the Cr leaching out after ADT, the Pt:Cr atomic ratio for the D-Pt_3Cr/C changes to approximately 6.5:1 and approximately 3.7:1 for the O-Pt_3Cr/C, clearly indicating that the ordered Pt_3Cr alloy is more stable than the disordered Pt_3Cr alloy, which is consistent with the results obtained in Figure 6.

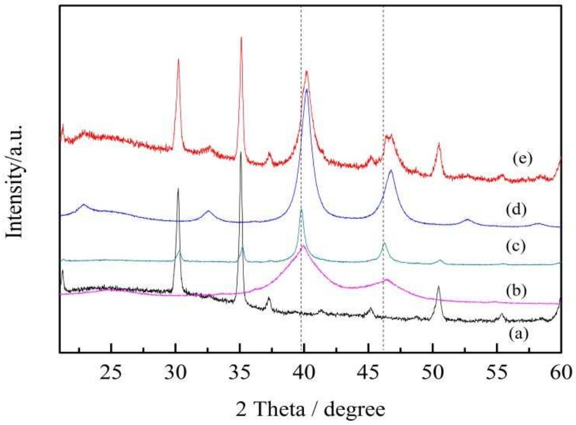

Fig. 7 XRD patterns of (a) ITO, (b) as-prepared D-Pt_3Cr/C, (c) D-Pt_3Cr/C+ITO after ADT, (d) as-prepared O-Pt_3Cr/C, and (e) O-Pt_3Cr/C+ITO after ADT

Figure 7 displays the XRD patterns of disordered and ordered Pt_3Cr/C electrocatalysts deposited on indium tin oxide (ITO) conductive glass before and after ADT. The dash lines in the figure are ascribed to pure Pt. The diffraction peaks of the D-Pt_3Cr/C sample after ADT shift to lower angles, which are very close to the peaks for pure Pt/C, strongly suggest the occurrence of de-alloying for the D-Pt_3Cr alloy nanoparticles. Except for the ITO peaks, two separated phases (Pt and ordered Pt_3Cr intermetallic compound) are clearly observed for the O-Pt_3Cr/C sample after ADT, similar to the reference[18], suggesting a possible Pt enrichment on the shell of the nanoparticles. The calculated mean particle size for the O-Pt_3Cr/C after ADT is 7.6 nm, which is only slightly larger than that of the as-prepared O-Pt_3Cr/C, and the mean particle size for the D-Pt_3Cr/C after ADT increases from 3.0nm to ca. 4.5 nm.

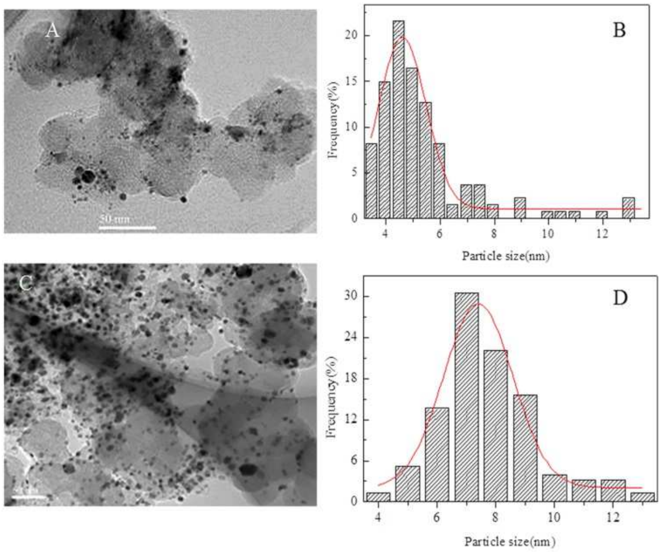

Fig. 8 TEM images (A, C) and their corresponding particle size distributions of (B, D) for D-Pt3Cr/C and O-Pt_3Cr/C after ADT.

TEM images of D-Pt_3Cr/C and O-Pt_3Cr/C after ADT are shown in Figure 8. For D-Pt_3Cr/C after ADT, some very large particles caused by the aggregation of small particles during the ADT are found. However, for the O-Pt_3Cr/C after ADT, the nanoparticles are still well distributed on the surface of carbon. The mean particle size is approximately 7.4 nm, which is only slightly larger than that of the as-prepared O-Pt_3Cr/C (as shown in Figure 2), again assessing that the good stability of the O-Pt_3Cr/C after the aggregation.

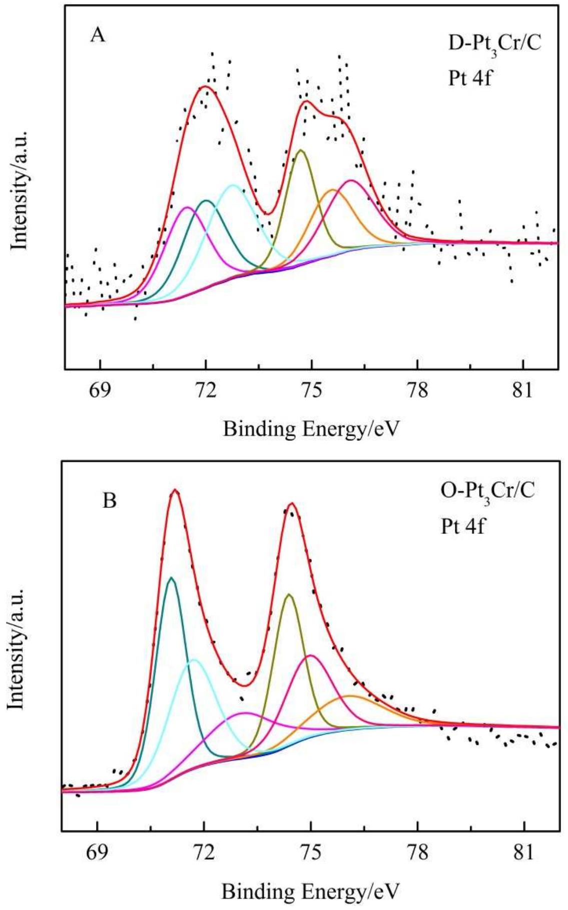

Fig. 9 XPS spectra of Pt 4f of D-Pt_3Cr/C (A) and O-Pt_3Cr/C (B) after ADT.

XPS analysis was also employed to explore the possible change in electronic properties after ADT, and the obtained results are shown in Figure 9 and Table 2. Compared with Figure 3, the BEs of Pt 4f for both D-Pt_3Cr/C and O-Pt_3Cr/C samples shift very slightly to lower BEs after ADT. The atomic proportions of Pt(0), Pt(II), and Pt(IV) are 31.6%, 30.6%, and 37.8%, respectively, for D-Pt_3Cr/C after ADT and 43.4%, 35.4%, and 21.2%, respectively, for O-Pt_3Cr/C after ADT. A lower decreased rate of Pt(0) demonstrates that the O-Pt_3Cr/C catalysts exhibits higher stability, which can be attributed to the greater chemical stability and corrosion resistance of the O-Pt_3Cr/C in acidic and oxidative environments.[39]

Conclusions

Carbon-supported Pt_3Cr intermetallic nanoparticles were successfully synthesized by structural transformation of disordered Pt_3Cr alloy. O-Pt_3Cr/C exhibits not only higher MA and SA but also much better durability toward the ORR than Pt/C. The change in ORR MA based on Pt decreases in the order of D-Pt_3Cr/C> O-Pt_3Cr/C> Pt/C-JM, whereas the ORR SA and durability increase in the order of Pt/C-JM< D-Pt_3Cr/C <<O-Pt_3Cr/C. The greatly enhanced durability of the O-Pt_3Cr/C catalyst for the ORR is caused by its improved structural stability. Thus, carbon-supported ordered Pt_3Cr nanoparticles can be considered as alternative cathode catalyst to improve the lifetime of the PEMFCs.

Acknowledgements

We would like to thank the National Basic Research Program of China (973 Program) (2012CB932800); Shanghai Science and Technology Committee (11DZ1200400, 12ZR1431200); the Knowledge Innovation Engineering of the CAS (12406, 124091231); and Drexel-SARI Global Funding Scheme for support to this work.

Notes and references

1. B. P. Vinayan, R. Nagar, N. Rajalakshmi and S. Ramaprabhu, *Adv Funct Mater*, 2012, **22**, 3519-3526.
2. A. Serov and C. Kwak, *Appl Catal B Environ*, 2009, **90**, 313-320.
3. R. Borup, J. Meyers, B. Pivovar, Y. S. Kim, R. Mukundan, N. Garland, D. Myers, M. Wilson, F. Garzon, D. Wood, P. Zelenay, K. More, K. Stroh, T. Zawodzinski, J. Boncella, J. E. McGrath, M. Inaba, K. Miyatake, M. Hori, K. Ota, Z. Ogumi, S. Miyata, A. Nishikata, Z. Siroma, Y. Uchimoto, K. Yasuda, K. Kimijima and N. Iwashita, *Chem Rev*, 2007, **107**, 3904-3951.
4. S. Sun, G. Zhang, D. Geng, Y. Chen, R. Li, M. Cai and X. Sun, *Angew Chem Int Ed*, 2011, **50**, 422-426.
5. D. Chen, X. Zhao, S. Chen, H. Li, X. Fu, Q. Wu, S. Li, Y. Li, B.-L. Su and R. S. Ruoff, *Carbon*, 2014, **68**, 755-762.
6. Q. Huang, H. Yang, Y. Tang, T. Lu and D. L. Akins, *Electrochem Commun*, 2006, **8**, 1220-1224.
7. E. R. Gonzalez, T. Lopes, E. Antolini and F. Colmati, *J Power Sources*, 2007, **164**, 111-114.
8. H. Yang, W. Vogel, C. Lamy and N. Alonso-Vante, *J Phys Chem B*, 2004, **108**, 11024-11034.
9. M. Ammam and E. B. Easton, *J Power Sources*, 2013, **236**, 311-320.
10. F. Taufany, C. J. Pan, H. L. Chou, J. Rick, Y. S. Chen, D. G. Liu, J. F. Lee, M. T. Tang and B. J. Hwang, *Chemistry*, 2011, **17**, 10724-10735.
11. J. H. Jang, E. Lee, J. Park, G. Kim, S. Hong and Y. U. Kwon, *Sci Rep*, 2013, **3**, 2872.
12. M. Oezaslan, F. Hasché and P. Strasser, *J Phys Chem Lett*, 2013, **4**, 3273-3291.
13. H. Li, H. Lin, Y. Hu, H. Li, P. Li and X. Zhou, *J Mater Chem*, 2011, **21**, 18447.
14. S. Mukerjee, *J Electrochem Soc*, 1995, **142**, 1409.
15. J. N. Tiwari, R. N. Tiwari, G. Singh and K. S. Kim, *Nano Energy*, 2013, **2**, 553-578.
16. H. Chen, D. Wang, Y. Yu, K. A. Newton, D. A. Muller, H. Abruna and F. J. DiSalvo, *J Am Chem Soc*, 2012, **134**, 18453-18459.

17. D. Wang, H. L. Xin, R. Hovden, H. Wang, Y. Yu, D. A. Muller, F. J. DiSalvo and H. D. Abruna, *Nat Mater*, 2013, **12**, 81-87.
18. S. Prabhudev, M. Bugnet, C. Bock and G. A. Botton, *ACS Nano*, 2013, **7**, 6103-6110.
19. X. Li, L. An, X. Wang, F. Li, R. Zou and D. Xia, *J Mater Chem*, 2012, **22**, 6047.
20. D. Xia, G. Chen, Z. Wang, J. Zhang, S. Hui, D. Ghosh and H. Wang, *Chem Mater*, 2006, **18**, 5746-5749.
21. B. M. Leonard, Q. Zhou, D. Wu and F. J. DiSalvo, *Chem Mater*, 2011, **23**, 1136-1146.
22. X. Wang, L. Altmann, J. Stöver, V. Zielasek, M. Bäumer, K. Al-Shamery, H. Borchert, J. Parisi and J. Kolny-Olesiak, *Chem Mater*, 2013, **25**, 1400-1407.
23. S. Maksimuk, S. Yang, Z. Peng and H. Yang, *J Am Chem Soc*, 2007, **129**, 8684-8685.
24. F. Matsumoto, C. Roychowdhury, F. J. DiSalvo and H. D. Abruna, *J Electrochem Soc*, 2008, **155**, B148-B154.
25. J. Shim, J. Lee, Y. Ye, J. Hwang, S. K. Kim, T. H. Lim, U. Wiesner and J. Lee, *ACS Nano*, 2012, **6**, 6870-6881.
26. Y. Kang, J. B. Pyo, X. Ye, T. R. Gordon and C. B. Murray, *ACS Nano*, 2012, **6**, 5642-5647.
27. C. Venkateswara Rao and B. Viswanathan, *J Phys Chem C*, 2009, **113**, 18907-18913.
28. C. V. Rao, A. L. M. Reddy, Y. Ishikawa and P. M. Ajayan, *Carbon*, 2011, **49**, 931-936.
29. H. Yang, N. Alonso-Vante, J. M. Leger and C. Lamy, *J Phys Chem B*, 2004, **108**, 1938-1947.
30. H. Yang, N. Alonso-Vante, C. Lamy and D. L. Akins, *J Electrochem Soc*, 2005, **152**, A704-A709.
31. L. Zou, J. Guo, J. Liu, Z. Zou, D. L. Akins and H. Yang, *J Power Sources*, 2014, **248**, 356-362.
32. H. Wei, L. Juanying, Q. Yongjin, Z. Zhiqing, Z. Xiaogang, D. L. Akins and Y. Hui, *J Power Sources*, 2010, **195**, 1046-1050.
33. X. Li, L. An, X. Chen, N. Zhang, D. Xia, W. Huang, W. Chu and Z. Wu, *Sci Rep*, 2013, **3**, 3234.
34. Z. Sun, Y. Zhao, Y. Xie, R. Tao, H. Zhang, C. Huang and Z. Liu, *Green Chem*, 2010, **12**, 1007.
35. W. Eberhardt, P. Fayet, D. M. Cox, Z. Fu, A. Kaldor, R. Sherwood and D. Sondericker, *Phys Rev Lett*, 1990, **64**, 780-783.
36. M. P. Hyman and J. W. Medlin, *J Phys Chem C*, 2007, **111**, 17052-17060.
37. W. He, M. Chen, Z. Q. Zou, Z. L. Li, X. G. Zhang, S. A. Jin, D. J. You, C. Pak and H. Yang, *Appl Catal B Environ*, 2010, **97**, 347-353.
38. Y. Dai, L. Ou, W. Liang, F. Yang, Y. Liu and S. Chen, *J Phys Chem C*, 2011, **115**, 2162-2168.
39. C. Yao, F. Li, X. Li and D. Xia, *J Mater Chem*, 2012, **22**, 16560.